Published in final edited form as:
Biomaterials. 2011 January ; 32(3): 808–818. doi:10.1016/j.biomaterials.2010.09.051.

Evaluation of Gel Spun Silk-Based Biomaterials in a Murine Model of Bladder Augmentation

Joshua R. Mauney[1,2], **Glenn M. Cannon Jr.**[1,2], **Michael L. Lovett**[3], **Edward M. Gong**[1,2], **Dolores DiVizio**[1,2], **David L. Kaplan**[3], **Rosalyn M. Adam**[1,2], and **Carlos R. Estrada Jr.**[1,2,*]

[1]Department of Urology, Urological Diseases Research Center, Children's Hospital Boston, Boston, MA, 02115, USA

[2]Department of Surgery, Harvard Medical School, Boston, MA, 02115, USA

[3]Department of Biomedical Engineering, Tufts University, Medford, MA, 02155, USA

Abstract

Currently, gastrointestinal segments are considered the gold standard for bladder reconstructive procedures. However, significant complications including chronic urinary tract infection, metabolic abnormalities, urinary stone formation, bowel dysfunction, and secondary malignancies are associated with this approach. Biomaterials derived from silk fibroin may represent a superior alternative due their robust mechanical properties, biodegradable features, and processing plasticity. In the present study, we evaluated the efficacy of a gel spun silk-based matrix for bladder augmentation in a murine model. Over the course of 70 d implantation period, H&E and Masson's trichrome (MTS) analysis revealed that silk matrices were capable of supporting both urothelial and smooth muscle regeneration at the defect site. Prominent uroplakin and contractile protein expression (α-actin, calponin, and SM22α) was evident by immunohistochemical analysis demonstrating maturation of the reconstituted bladder wall compartments. Gel spun silk matrices also elicited a minimal acute inflammatory reaction following 70 d of bladder integration, in contrast to parallel assessments of small intestinal submucosa (SIS) and polyglycolic acid (PGA) matrices which routinely promoted evidence of fibrosis and chronic inflammatory responses. Voided stain on paper analysis revealed that silk augmented animals displayed similar voiding patterns in comparison to non surgical controls by 42 d of implantation. In addition, cystometric evaluations of augmented bladders at 70 d post-op demonstrated that silk scaffolds supported significant increases in bladder capacity, voided volume, and flow rate while maintaining similar degrees of compliance relative to the control group. These results provide evidence for the utility of gel spun silk-based matrices for functional bladder tissue engineering applications.

Keywords

silk; bladder tissue engineering; smooth muscle cell; SIS; Polyglycolic acid

INTRODUCTION

The urinary bladder functions to store urine at low pressures and expel it under voluntary control. In various congenital and acquired disorders, the urinary tract is anatomically or functionally obstructed resulting in elevated risk for incontinence and kidney damage due to increased storage and voiding pressures. These conditions include posterior urethral valves,

*Corresponding author: Carlos Estrada, M.D., Children's Hospital Boston, Department of Urology, 300 Longwood Ave., Hunnewell 3, Boston, MA 02115; Phone: 617-355-3338; Fax: 617-730-0474; carlos.estrada@childrens.harvard.edu.

neurogenic bladder secondary to spina bifida or spinal cord injury, benign prostatic hyperplasia, bladder and cloacal exstrophy, and severe voiding dysfunction [1]. The urinary tract can also be compromised by malignancy, most commonly transitional cell carcinoma [2]. Surgical treatment of these pathologies requires bladder augmentation in the case of obstructive diseases [3], or organ substitution following radical cystectomy for bladder cancer [4]. Currently, gastrointestinal segments including stomach, colon, and ileum are considered the gold standard for bladder reconstructive procedures [5]. However, significant complications including chronic urinary tract infection, metabolic abnormalities, urinary stone formation, bowel dysfunction, and secondary malignancies are associated with this approach [6,7].

To address these limitations and complications, bladder tissue engineering efforts have been aimed at deployment of a biocompatible scaffold capable of facilitating tissue regeneration. In order for complete bladder repair to occur, biomaterial configurations must support reconstitution of both the smooth muscle compartment as well as the urothelium to restore organ contractile and permeability functions, respectively [8,9]. Previous studies have investigated the use of natural polymers such as small intestine submucosa (SIS) and bladder acellular matrix (BAM) as alternative biomaterials for bladder regeneration [10,11]. Although these biomaterials contain endogenous growth factors and extracellular matrix cues which can enhance and accelerate defect healing [12,13], limitations in terms of their mechanical integrity and biocompatibility often result in deleterious fibrosis [14], graft contracture [15] and calcification [16]. Biodegradable synthetic polymers such as those derived from poly-glycolic acid (PGA) and/or poly-lactic acid (PLA) have been reported to support *de novo* urothelial and smooth muscle tissue formation as well as preserve renal function following bladder integration [8,17]. Unfortunately, these matrices elicit relatively strong inflammatory responses in vivo with the potential to retard defect consolidation and contribute to implant failure [18]. These limitations apply to both cell seeded and non-cell seeded biomaterial scaffolds, and whether cell seeding is ultimately necessary is an unanswered question. In either case, current biomaterials have demonstrated significant limitations, and there exists a critical need to develop and investigate novel scaffolds better suited to bladder functionality.

Polymeric systems derived from silk fibroin may serve as a potential option for use in bladder repair strategies. Silk-based biomaterials have been used previously in diverse tissue engineering applications including regeneration of musculoskeletal tissues and certain hollow organs [19,20]. Plasticity in terms of silk processing methods allows for the construction of a variety of biodegradable [21] biomaterial configurations including films [22], foams [23], electrospun nanofibers [24], hydrogels [25], and woven and non woven meshes [26]. In particular, the process of gel spinning has been demonstrated to generate multi-laminate matrices organized from shear-induced fibers of aquesous silk fibroin [27]. This process allows for precise control over scaffold architecture, porosity, and composite features [27]. Gel spun silk matrices exhibit an exceptional combination of physical characteristics such as high tensile strength and degree of elasticity [27] that are potentially well suited to support bladder function. In the present study, we investigated the utility of non-cell seeded gel spun silk matrices in a murine model of bladder augmentation. Urodynamic and histological parameters were evaluated and compared with the performance of conventional augment biomaterials, PGA and SIS.

MATERIALS AND METHODS

Biomaterials

Silk tubes were formed using a previously described gel spinning technique [27]. Briefly, aqueous silk fibroin solutions were prepared from *Bombyx mori* silkworm cocoons using

previously described procedures [28]. Tubes were then produced by spinning concentrated silk solutions (~25–40% (w/v) onto a rotating and axially reciprocating mandrel (6 mm in diameter). Using the custom gel spinning platform and program, tubes were spun at a rotational speed of 200 rpm and an axial speed of 2 mm/s. A 25G needle was used to spin 6–8 layers of silk onto the mandrel, before treating the tube with methanol to induce the transformation from amorphous liquid to the β-form silk fibroin conformation characterized by anti-parallel β-sheets [29]. The tube was then removed from the mandrel after briefly soaking in a surfactant solution. Tubular scaffolds were then bisected along their central axis, sterilized in 70% ethanol, rinsed in PBS, and subjected to surgical procedures detailed below. 3-D poly-glycolic acid woven meshes (PGA) (Concordia Fibers, Coventry, RI) and small intestine submucosa (SIS) (Cook Medical Inc., Bloomington, IN) scaffolds were evaluated in parallel as standard points of comparison since these biomaterials have been previously deployed in bladder augmentation approaches in both animal and human models [10,17].

Murine Bladder Augmentation

Biomaterials were evaluated in a bladder augmentation model utilizing an immunocompetent mouse strain (CD1, 6 weeks, 22–24g, Jackson Laboratories, Bar Harbor, ME) following IACUC approved protocols. A schematic of the various surgical stages performed during this procedure is detailed in Figure 1. Briefly, animals were anesthetized using isoflurane inhalation and then shaved to expose the surgical site. A low midline laparotomy incision was then made and the underlying tissue (rectus muscle and peritoneum) was dissected free to expose the bladder. The anterior portion (immediately distal to the dome) of the bladder where the tissue construct was incorporated was marked with 7-0 nylon sutures in a square (1 cm^2) configuration. These sutures were used as holding sutures for the anastomosis of the biomaterials. A 1 cm^2 bladder defect was then created with fine scissors by cutting immediately inside of the holding sutures. Biomaterials were then integrated into the bladder defect using 7-0 polyglactin (Vicryl) continuous suture. A watertight seal was confirmed by filling the bladder with sterile saline via instillation through a 30 gauge hypodermic needle. Local injection of bupivicaine into the rectus muscle and subcutaneous tissue (<3 mg/kg of 0.25%) was administered during the closure. A total of 17 silk-based implants, 7 PGA matrices, and 6 SIS scaffolds were assessed independently for up to 70 d of implantation. At selected time points, animals were subjected to voided stain on paper (VSOP), cystometric, and/or histological analyses (Table 1). A total of 12 non surgical control animals of equal size and weight were assessed in parallel.

VSOP Analysis

Conscious voiding function was studied utilizing a Voiding Stain on Paper technique previously described [30]. At 42 d of scaffold implantation, VSOP was used to analyze voided volume, voiding frequency, and voiding pattern. Mice were housed individually in metabolic cages for three hours between 2:00pm and 6:00pm with food pellets and water readily available. Cellulose filter paper (Whatman International Ltd, Grade 1) cut to 25 cm diameter was placed underneath the mesh floor of the cages to catch urinary voids. Voiding pattern was analyzed using an ultraviolet bioimaging system (Chemigenius^{2,} Syngene, Cambridge, UK). In order to calculate VSOP parameters, a calibration curve was generated using defined (Ward's Natural Science, Rochester, NY) and stained area on filter paper.

Murine Cystometric Analysis

Murine cystometric analyses were performed utilizing an open abdominal technique. Mice were anesthetized with intraperitoneal ketamine. A 1cm lower-midline incision was made and the bladder identified. The bladder was accessed with a 27G needle attached to a pressure transducer (ADInstruments, Colorado Springs, CO) and a Harvard 22 syringe pump

(Harvard Apparatus, Holliston, MA). The pressure transducer was calibrated with a mercury manometer. Room temperature saline was infused at a rate of 1 ml/hr. Data was collected with a Bridge Amp and a Power Lab 4/30 (ADInstruments, Colorado Springs, CO) and analyzed with Lab Chart 6 (ADInstruments). After establishment of a regular voiding pattern, bladder compliance was determined by dividing the change in bladder pressure during filling over time between voids. Average peak voiding pressure was determined by the cystometrographic results. Saline was collected with each void and mean flow rate was determined by dividing the volume voided by the time for each individual void. Post-void residual was determined by bladder aspiration after voiding. Total bladder capacity was determined by adding voided volume to post-void residual. A total of 4 voiding cycles were analyzed per mouse to determine urodynamic parameters. Data for these measurements were analyzed by ANOVA with post-hoc Bonferroni testing using commercially available statistical software (StatPlus:mac 2008, AnalystSoft, Vancouver, BC). Statistically significant values were defined as $p<0.05$.

Histological and Immunohistochemical Analyses

Following various implantation periods, animals were euthanized by CO_2 asphyxiation and bladders were excised for standard histological processing. Briefly, organs were fixed in 10% neutral-buffered formalin, dehydrated in graded alcohols, and then embedded in paraffin in an axial orientation to capture the entire circumferential surface of the bladder with each section. Correct orientation (anterior vs posterior) within the paraffin block was determined by suture placement on the specimen. Sections (10 μm) were cut and then stained with hematoxylin and eosin or Masson's trichrome as previously described [31]. For immunohistochemical analysis, contractile smooth muscle markers such as α-actin, SM22α, and calponin as well as urothelial-associated proteins, uroplakins, were detected using the following primary antibodies: anti-α-actin [Sigma-Aldrich, St. Louis, MO, cat.# A2457, 1:200 dilution] anti-SM22α [Abcam, Cambridge, MA, cat.# ab14106, 1:200 dilution], anti-calponin [Sigma Aldrich, cat.# C2687, 1:250] and pan-uroplakin [rabbit antisera raised against total bovine uroplakin extracts, a gift from TT Sun from New York University, 1:250 dilution] followed by incubation with species-matched Cy3-conjugated secondary antibodies (Millipore, Billerica, MA). Nuclei were counterstained with 4', 6-diamidino-2-phenyllindole (DAPI), and specimens were visualized using a Nikon Eclipse TE2000-U fluorescence microscope (Nikon Instruments Inc., Melville, NY).

RESULTS

Over the course of the 70 d implantation period, survival rates of the augmented animals varied between the scaffold groups prior to scheduled euthanasia. Bladder reconstruction with silk resulted in an 82% survival rate, similar to the 71% observed with PGA augmented animals, but substantially higher than SIS implants which exhibited only a 66% survival rate. A total of seven mice augmented with either silk (3), SIS (2), or PGA (2) died within the first post operative week. Post mortem analysis revealed urinary ascites as the probable cause of death in all animals examined except 1 silk augmented animal, which exhibited a bowel obstruction. Evidence of either scaffold perforation or dehiscence at the suture line between the implant and the native bladder wall was noted in all of subjects where urinary ascites was evident. The remaining augmented animals had an uneventful post-operative period. At the time of planned euthanasia, no signs of bladder calculi or mucus were observed within the implant groups following macroscopic examination.

The extent of bladder regeneration in augmented bladders was determined by hematoxylin and eosin (H&E) (Figure 2) and Masson's trichrome (MTS) analysis (Figure 3). By 21 d, substantial connective tissue ingrowth from the border of the native bladder wall was evident along the periphery of the silk matrix and traversed the original defect site. The

regenerated tissue was lined with a luminal transitional epithelium bordered by a lamina propria populated by fibroblastic cell populations. This compartment exhibited minimal eosin and MTS staining compared to the non surgical control reflecting sparse extracellular matrix (ECM) deposition potentially due to an immature state of repair. The presence of smooth muscle bundles was also evident around the outer layer of the consolidated tissue (pink: H&E; red: MTS); however at this point of regeneration, they were primarily concentrated at the border of surgical integration. The pattern of host tissue integration into the defect area varied among group replicates wherein 66% displayed entrapment of the silk matrix within the smooth muscle and lamina propria compartments (data not shown) while 33% exhibited a luminal orientation. Morphological characteristics of the bladder wall compartments were similar regardless of the orientation of the silk matrix within the regenerated tissue.

After 70 d post-op, higher levels of eosin (pink) and MTS (pink) staining were observed within the lamina propria of the regenerated tissue supported by the silk matrix indicating increases in ECM deposition in comparison to the 21 d group. The presence of smooth muscle bundles traversing the entire width of the defect site was also evident by prominent MTS staining (red), potentially reflecting a continued maturation of the regenerated tissue. The bulk of the silk matrices were still intact within defect sites following 70 d of implantation, however focal points of macrophage infiltration and scaffold fragmentation were observed among group replicates (Figure 4). The distribution pattern of the silk implants located within the bladder wall or lumen was similar to the results observed in the 21 d group. A minimal acute inflammatory reaction was also noted at this time point by the presence of disperse eosinophil granulocytes bordering the silk implants (Figure 4). However, no evidence of a chronic inflammatory response or fibrosis was observed in this group.

Histological analysis of bladders augmented with SIS following 70 d of implantation demonstrated consolidation of the defect site with dense connective tissue (Figures 2 and 3). The regenerated tissue exhibited a transitional epithelium similar in morphology to that observed in silk augmented bladders and nonsurgical controls. Bladder wall components consisted of an ECM-rich lamina propria populated with fibroblastic cells as well as a smooth muscle layer organized into bundles transversing the width of the original defect site. However, high levels of MTS staining (blue) were observed in the regenerated tissue dispersed between the smooth muscle fibers possibly indicative of fibrotic tissue (Figure 3). In contrast with the results observed with the silk scaffolds, the thickness of the SIS-mediated regenerated tissue was diminished in comparison to the residual native bladder wall. A mild chronic inflammatory reaction was also noted within the SIS augmented bladder wall consisting of aggregates of mononuclear cells mobilized to the implantation site (Figure 4).

In contrast to the results observed with silk, the extent of urothelial regeneration supported by the PGA scaffolds was much less developed, demonstrating hypoplastic basal and intermediate cell layers (Figures 2 and 3). In addition, the regenerated lamina propria and smooth muscle compartments supported by the PGA implants displayed higher levels of MTS (blue) staining and a more disorganized structure of ECM deposition indicative of fibrotic tissue formation (Figure 3). A severe chronic inflammatory reaction was noted among PGA replicates demonstrating a foreign body response exemplified by the presence of multi-nuclear giant cells encapsulating the scaffold remnants within the bladder wall (Figure 4). In contrast to the silk implants, the majority of the SIS and PGA matrices showed evidence of substantial degradation within the bladder wall, but residual matrix fragments were also dispersed predominantly within the lumen (Figures 2 and 3).

Immunohistochemical analysis revealed that over the course of the 70 d implantation period silk matrices supported a gradual progression of urothelial (Figure 5) and smooth muscle maturation (Figure 6). By 21 d post-op, the regenerated tissue displayed a transitional epithelium exhibiting prominent luminal uroplakin staining which increased in intensity and distribution throughout the basal and intermediate cell layers by 70 d of implantation. Similar levels of uroplakin staining were also observed throughout the urothelium of the regenerated tissue supported by the SIS. In contrast to the SIS and silk, uroplakin staining was disperse and discontinuous in the *de novo* urothelium facilitated by the PGA implants.

Our results also showed that smooth muscle bundles located on the periphery of the regenerated tissue supported by the silk implants stained positive for α-actin and SM22α protein expression, but predominantly negative for calponin following 21 d of implantation. By 70 d post-op, regenerated tissue supported by the silk matrix contained dense smooth muscle bundles traversing the entire width of the implant and exhibiting positive staining for α-actin, SM22α, and calponin. Similar degrees of contractile marker staining and distribution were observed within the SIS augmented bladders in comparison to the silk group at this time point. *De novo* tissue supported by the PGA implants exhibited smooth muscle bundles positive for α-actin protein expression, however SM22α and calponin expression was confined to dispersed submucosal fibroblastic populations. The formation of circular vessel structures positive for α-actin expression was detected within the regenerated tissue supported by silk implants following 21 d post-op and all three matrix groups at 70 d of implantation.

Functional analysis of augmented bladders was assessed by VSOP at 42 d of implantation. There was a linear correlation between liquid volume and stained area on the filter paper within the range of 25–300 μl (Figure 7A, $y = 0.125x + 0.898$, $R^2 = 0.9979$). Mice augmented with each scaffold type displayed voiding patterns similar to non surgical controls wherein micturition primarily occurred around the periphery of the filter paper (Figure 7B). The frequency of voids generated by the bladders implanted with silk was similar to the levels observed in the PGA group, but substantially higher than those observed in both the non surgical controls and SIS implants (Figure 7C). The amount of urine per void was similar in the non surgical controls, silk and PGA augmented bladders while the SIS implanted group displayed considerable increases in voided volume (Figure 7D). Following 70 d of biomaterial implantation, cystometric analysis was also performed in order to assess the extent of organ function (Figure 8A and B). The degree of compliance of the silk augmented bladders was found to be statistically similar to non surgical controls, while bladders repaired with SIS and PGA scaffolds displayed substantially attenuated levels by comparison. Bladder capacity and voided volumes significantly increased in all augmented groups in comparison to non surgical controls with animals implanted with silk displaying the highest levels of both parameters. In addition, silk augmented bladders exhibited significant increases in voiding flow rate in comparison to all other augmented groups and control animals.

DISCUSSION

Maintenance of urinary tract health is crucially dependent on the voiding and storage capacities of the urinary bladder. To treat a number of acquired and congenital abnormalities, bladder augmentation is needed to increase organ capacity thereby reducing elevated storage pressures and preserving renal function and continence. Limitations in conventional biomaterials utilized for bladder wall replacement prompted our investigation into the efficacy of silk fibroin-based matrices as a potential alternative.

Traditionally, the use of silk sutures in bladder reconstruction has been associated with deleterious consequences including inflammation [32] and urinary calculi [33]. Various commercialgrade sutures, however, are composed of raw silk fibers [19,34] which are known to contain sericin, a residual glue-like protein which constitutes the major antigenic properties of silk [35–38]. In the present study, processing steps inherent to the production of soluble silk fibroin used during the gel spinning technique minimizes the presence of sericin through the use of repetitive washing cycles with sodium carbonate solution [35,39,40]. Histological observations of the defect site augmented with gel spun silk matrices demonstrated a mild acute inflammatory reaction, but no evidence of foreign body response or urinary stone formation. These features are in stark contrast to silk sutures which routinely elicit this type of chronic inflammatory reaction resulting in implant calcification [33].

The results of the present study demonstrate the potential of gel spun silk scaffolds to support murine bladder tissue regeneration. In comparison to conventional matrices such as SIS and PGA, survival rates of animals following silk implantation showed lower degrees of morbidity associated with the procedure. Since premature death following biomaterial incorporation was routinely associated with urinary ascites due to scaffold perforation or dehiscence at the integration site, these data suggest that gel spun silk configurations may offer an advantage over conventional biomaterials due their ability to support increased mechanical stability of the defect site. Although rupture of augmented bladders has a relatively low rate of incidence following enterocystoplasty in patients at approximately 8.6% according to a study by Metcalfe and colleagues [41], this complication represents a serious and life-threatening issue. Therefore the deployment of biomaterial designs which can minimize this risk, such as the silk matrices described here, may be of potential clinical value.

Histological and immunohistochemical analysis revealed that silk scaffolds were capable of supporting urothelial formation and maturation along the defect site. By 21 d of implantation, the formation of a transitional urothelium lining the lumen of the regenerated tissue was noted with a gradual increase in the degree and distribution of uroplakin expression up to 70 d following implantation. These results were comparable to non surgical controls and SIS augmented bladders. The presence of urothelium at defect sites has been reported to occur within 2 to 4 weeks following SIS bladder augmentation in a variety of animal models [42,43]. Uroplakin expression and subsequent asymmetrical unit membrane formation is essential for the maintenance of the urothelial permeability barrier [44]. The ability of silk scaffolds to support host tissue re-epithelialization of the defect site represents a critical feature of this biomaterial configuration for use in bladder reconstructive procedures. In comparison to PGA augmented bladders, silk scaffolds demonstrated a more robust and continuous urothelial layer. Chronic inflammatory responses, as noted in the PGA implants, are known to attenuate uroplakin expression and disrupt barrier function [45] and therefore their presence may explain the results seen in the present study.

Silk matrices also supported *de novo* formation of a lamina propria and smooth muscle layer within the defect site. Maturation of the smooth muscle compartment was evident with α-actin and SM22α expression at the periphery of the silk implant by 21 d with a progression to thick smooth muscle bundles traversing the defect site and displaying robust calponin expression by 70 d post-op. The ability of smooth muscle cells to mediate voiding functions of the urinary bladder is intimately dependent on their expression of contractile protein machinery [46.47]. In comparison to silk scaffolds, the SIS regenerated tissue contained smooth muscle bundles stained similarly for contractile proteins, however evidence of fibrosis and an attenuated width suggested an immature state of repair. Previous studies have reported smooth muscle bundle formation in SIS augmented bladders between 8–12 weeks

of implantation depending on the model system [42,43], results consistent with observations in the present study.

In comparison to silk matrices, the smooth muscle compartment reconstituted by the PGA augments displayed smooth muscle bundles expressing α-actin, however SM22α and calponin expression was localized to submucosal cell populations surrounding fibrotic tissue indicative of the presence of myofibroblasts at the defect site [48,49]. The reduced width of the regenerated tissue may also reflect the immature state of repair supported by the PGA implants in comparison to the silk matrices. The exact mechanisms of bladder smooth muscle regeneration supported by silk scaffolds are currently unknown. However, previous studies have demonstrated that restoration is linked to epithelial interactions, transdifferentiation of fibroblasts into phenotypic SMCs, or dedifferentiation and migration of peripheral SMCs from the host bladder wall into the defect site [50–52]. Future studies will focus on identifying the crucial regulatory processes responsible for promoting bladder tissue formation following augmentation.

A relatively slow rate of silk scaffold resorption was observed in comparison to SIS and PGA implants. Slow scaffold resorption can increase the risk of urinary stone formation over time [53]. However, the rapid rate of SIS and PGA degradation may have contributed to the relatively immature state of repair due to insufficient mechanical support during ingrowth of bladder wall components into the defect site. Future long-term studies will be required to verify the ability of silk scaffolds to completely degrade and be fully replaced with *de novo* host tissue. Adjustments in gel spinning post-winding parameters to include lyophilization may be a potential option to enhance tissue infiltration and degradation due its ability to promote increased degrees of porosity within the scaffold architecture [27].

VSOP analysis of augmented bladders at 42 d of implantation demonstrated differences in the voluntary voiding patterns between each of the matrix groups. Animals implanted with SIS voided less often and with more volume per void in comparison to non surgical controls, consistent with an increased degree of bladder capacity. Mice augmented with PGA had higher numbers of voids per analysis period with similar amounts of voided volume in comparison to controls. Previous studies have demonstrated a positive correlation between increases in voiding frequency and the disruption of the urothelial permeability barrier [54]. Since histological analysis revealed an incomplete state of urothelial regeneration at 70 d post-op in PGA augmented bladders, this feature may be responsible for the increased level of voids observed at this earlier time point. Voiding patterns for silk augmented bladders were similar to the results obtained with the PGA group and therefore may also reflect an immature state of urothelial repair at this stage of regeneration.

The “gold standard” of recovery following bladder augmentation is a regenerated organ which displays (**1**) increases in bladder capacity sufficient to preserve renal function and continence, (**2**) bladder wall compliance comparable to non-diseased counterparts to allow for adequate elasticity for voiding and urine storage, and in appropriate patients, (**3**) a non occluded urinary outlet which allows for sufficient evacuation during micturition. Cystometric evaluations of the various bladder augment groups revealed significantly different degrees of functional performance based on the evaluation of several urodynamic parameters at 70 d post-op. Compliance levels of silk augmented bladders were found to be comparable to the non surgical control group. These results are consistent with the extent of structural organization and maturation of bladder wall components seen histologically and immunohistochemically in parallel analyses. By comparison, the low degree of compliance exhibited by the PGA and SIS augmented bladders is in agreement with the presence of fibrotic tissue remodeling and the immature state of the regenerated tissue observed histologically at this phase of implantation. While all matrix groups demonstrated increases

in bladder capacity as well as voided volume in comparison to control animals, silk augmented bladders displayed the highest extent, possibly reflecting the increased compliance exhibited by the regenerated tissue. In addition, urinary flow rates showed a similar trend, wherein silk augmented bladders displayed the highest level over all other matrix groups. This feature is potentially due to the enhanced degree of tissue regeneration and maturation observed following silk implantation in comparison to augmentation with PGA and SIS matrices.

CONCLUSIONS

The results presented in this study provide the first evidence for the feasibility of gel spun silk matrices in bladder augmentation procedures. These scaffolds supported urothelial and smooth muscle regeneration and also led to increases in bladder capacity and voided volume in a murine model. In comparison to conventional augment matrices such as PGA and SIS, silk scaffolds demonstrated significant advantages including decreased animal mortality, enhanced tissue regeneration, lack of chronic inflammatory reactions, and improvements in functional performance. Future studies will focus on evaluating the utility of silk-based biomaterials in large animal models of bladder reconstruction.

Acknowledgments

The authors wish to thank Esha Mathew, MSc. for her technical assistance as well as Dr T.T. Sun for his kind gift of the anti-pan-uroplakin antibody.

ROLE OF THE FUNDING SOURCE

Tissue Engineering Resource Center, NIBIB P41 EB002520 (KAPLAN); Children's Hospital Boston Office of Sponsored Programs Support for Pilot Studies (ESTRADA); NIDDK P50 DK065298-06 (FREEMAN); Harvard Catalyst/The Harvard Clinical and Translational Science Center NIH UL1 RR 025758 (ESTRADA).

REFERENCES

1. Atala A. Tissue engineering for bladder substitution. World J Urol. 2000; 18(5):364–370. [PubMed: 11131316]
2. Cho KS, Seo JW, Park SJ, Lee YH, Choi YD, Cho NH, et al. The risk factor for urethral recurrence after radical cystectomy in patients with transitional cell carcinoma of the bladder. Urol Int. 2009; 82(3):306–311. [PubMed: 19440019]
3. Hatch DA, Koyle MA, Baskin LS, Zaontz MR, Burns MW, Tarry WF, et al. Kidney transplantation in children with urinary diversion or bladder augmentation. J Urol. 2001; 165(6):2265–2268. [PubMed: 11371960]
4. Hautmann RE. Which patients with transitional cell carcinoma of the bladder or prostatic urethra are candidates for an orthotopic neobladder? Curr Urol Rep. 2000; 1(3):173–179. [PubMed: 12084311]
5. Niknejad KG, Atala A. Bladder augmentation techniques in women. Int Urogynecol J Pelvic Floor Dysfunct. 2000; 11(3):156–169. [PubMed: 11484743]
6. Somani BK, Kumar V, Wong S, Pickard R, Ramsay C, Nabi G, et al. Bowel dysfunction after transposition of intestinal segments into the urinary tract: 8-year prospective cohort study. J Urol. 2007; 177(5):1793–1798. [PubMed: 17437822]
7. Hensle TW, Gilbert SM. A review of metabolic consequences and long-term complications of enterocystoplasty in children. Curr Urol Rep. 2007; 8(2):157–162. [PubMed: 17303022]
8. Jack GS, Zhang R, Lee M, Xu Y, Wu BM, Rodríguez LV. Urinary bladder smooth muscle engineered from adipose stem cells and a three dimensional synthetic composite. Biomaterials. 2009; 30(19):3259–3270. [PubMed: 19345408]
9. Roth CC, Kropp BP. Recent advances in urologic tissue engineering. Curr Urol Rep. 2009; 10(2): 119–125. [PubMed: 19239816]

10. Kropp BP. Small-intestinal submucosa for bladder augmentation: a review of preclinical studies. World J Urol. 1998; 16(4):262–267. [PubMed: 9775425]
11. Obara T, Matsuura S, Narita S, Satoh S, Tsuchiya N, Habuchi T. Bladder acellular matrix grafting regenerates urinary bladder in the spinal cord injury rat. Urology. 2006; 68(4):892–897. [PubMed: 17070388]
12. Nihsen ES, Johnson CE, Hiles MC. Bioactivity of small intestinal submucosa and oxidized regenerated cellulose/collagen. Adv Skin Wound Care. 2008; 21(10):479–486. [PubMed: 18836327]
13. Azzarello J, Ihnat MA, Kropp BP, Warnke LA, Lin HK. Assessment of angiogenic properties of biomaterials using the chicken embryo chorioallantoic membrane assay. Biomed Mater. 2007; 2(2):55–61. [PubMed: 18458436]
14. Boruch AV, Nieponice A, Qureshi IR, Gilbert TW, Badylak SF. Constructive Remodeling of Biologic Scaffolds is Dependent on Early Exposure to Physiologic Bladder Filling in a Canine Partial Cystectomy Model. J Surg Res. 2009; 161(2):217–225. [PubMed: 19577253]
15. Brown AL, Farhat W, Merguerian PA, Wilson GJ, Khoury AE, Woodhouse KA. 22 week assessment of bladder acellular matrix as a bladder augmentation material in a porcine model. Biomaterials. 2002; 23(10):2179–2190. [PubMed: 11962659]
16. van Wachem PB, van Luyn MJ, Olde Damink LH, Dijkstra PJ, Feijen J, Nieuwenhuis P. Biocompatibility and tissue regenerating capacity of crosslinked dermal sheep collagen. J Biomed Mater Res. 1994; 28(3):353–363. [PubMed: 8077250]
17. Atala A, Bauer SB, Soker S, Yoo JJ, Retik AB. Tissue-engineered autologous bladders for patients needing cystoplasty. Lancet. 2006; 367(9518):1241–1246. [PubMed: 16631879]
18. Ceonzo K, Gaynor A, Shaffer L, Kojima K, Vacanti CA, Stahl GL. Polyglycolic acid-induced inflammation: role of hydrolysis and resulting complement activation. Tissue Eng. 2006; 12(2): 301–308. [PubMed: 16548688]
19. Altman GH, Diaz F, Jakuba C, Calabro T, Horan RL, Chen J, et al. Silk-based biomaterials. Biomaterials. 2003; 24(3):401–416. [PubMed: 12423595]
20. Wang Y, Kim HJ, Vunjak-Novakovic G, Kaplan DL. Stem cell-based tissue engineering with silk biomaterials. Biomaterials. 2006; 27(36):6064–6082. [PubMed: 16890988]
21. Wang Y, Rudym DD, Walsh A, Abrahamsen L, Kim HJ, Kim HS, et al. In vivo degradation of three-dimensional silk fibroin scaffolds. Biomaterials. 2008; 29(24–25):3415–3428. [PubMed: 18502501]
22. Gil ES, Park SH, Marchant J, Omenetto F, Kaplan DL. Response of Human Corneal Fibroblasts on Silk Film Surface Patterns. Macromol Biosci. 2010; 10(6):664–673. [PubMed: 20301120]
23. Nazarov R, Jin HJ, Kaplan DL. Porous 3-D scaffolds from regenerated silk fibroin. Biomacromolecules. 2004; 5(3):718–726. [PubMed: 15132652]
24. Wadbua P, Promdonkoy B, Maensiri S, Siri S. Different properties of electrospun fibrous scaffolds of separated heavy-chain and light-chain fibroins of Bombyx mori. Int J Biol Macromol. 2010; 46(5):493–501. [PubMed: 20338193]
25. Kluge JA, Rosiello NC, Leisk GG, Kaplan DL, Dorfmann AL. The consolidation behavior of silk hydrogels. J Mech Behav Biomed Mater. 2010; 3(3):278–289. [PubMed: 20142112]
26. Min BM, Jeong L, Nam YS, Kim JM, Kim JY, Park WH. Formation of silk fibroin matrices with different texture and its cellular response to normal human keratinocytes. Int J Biol Macromol. 2004; 34(5):223–230. [PubMed: 15374678]
27. Lovett ML, Cannizzaro CM, Vunjak-Novakovic G, Kaplan DL. Gel spinning of silk tubes for tissue engineering. Biomaterials. 2008; 29(35):4650–4657. [PubMed: 18801570]
28. Kim UJ, Park J, Kim HJ, Wada M, Kaplan DL. Three-dimensional aqueous-derived biomaterial scaffolds from silk fibroin. Biomaterials. 2005; 26(15):2775–2785. [PubMed: 15585282]
29. Wang X, Kim HJ, Xu P, Matsumoto A, Kaplan DL. Biomaterial coatings by stepwise deposition of silk fibroin. Langmuir. 2005; 21(24):11335–11341. [PubMed: 16285808]
30. Sugino Y, Kanematsu A, Hayashi Y, Haga H, Yoshimura N, Yoshimura K, et al. Voided stain on paper method for analysis of mouse urination. Neurourol Urodyn. 2208; 27(6):548–552. [PubMed: 18551561]

31. Kropp BP, Rippy MK, Badylak SF, Adams MC, Keating MA, Rink RC, et al. Regenerative urinary bladder augmentation using small intestinal submucosa: urodynamic and histopathologic assessment in long-term canine bladder augmentations. J Urol. 1996; 155(6):2098–2104. [PubMed: 8618344]
32. Imamoglu M, Cay A, Sarihan H, Ahmetoglu A, Ozdemir O. Paravesical abscess as an unusual late complication of inguinal hernia repair in children. J Urol. 2004; 171(3):1268–1270. [PubMed: 14767328]
33. Shimamura T, Strauss G. Reactions to vesical foreign bodies in two strains of rats. Jpn J Exp Med. 1988; 58(1):9–13. [PubMed: 3288786]
34. Soong HK, Kenyon KR. Adverse reactions to virgin silk sutures in cataract surgery. Ophthalmology. 1984; 91(5):479–483. [PubMed: 6377167]
35. Meinel L, Hofmann S, Karageorgiou V, Kirker-Head C, McCool J, Gronowicz G, et al. The inflammatory responses to silk films in vitro and in vivo. Biomaterials. 2005; 26(2):147–155. [PubMed: 15207461]
36. Dewair M, Baur X, Ziegler K. Use of immunoblot technique for detection of human IgE and IgG antibodies to individual silk proteins. J Allergy Clin Immunol. 1985; 76(4):537–542. [PubMed: 4056241]
37. Wen CM, Ye ST, Zhou LX, Yu Y. Silk-induced asthma in children: a report of 64 cases. Ann Allergy. 1990; 65(5):375–378. [PubMed: 2244708]
38. Zaoming W, Codina R, Fernandez-Caldas E, Lockey RF. Partial characterization of the silk allergens in mulberry silk extract. J Investig Allergol Clin Immunol. 1996; 6(4):237–241.
39. Altman GH, Horan RL, Lu HH, Moreau J, Martin I, Richmond JC, et al. Silk matrix for tissue engineered anterior cruciate ligaments. Biomaterials. 2002; 23(20):4131–4141. [PubMed: 12182315]
40. Sofia S, McCarthy MB, Gronowicz G, Kaplan DL. Functionalized silk-based biomaterials for bone formation. J Biomed Mater Res. 2001; 54(1):139–148. [PubMed: 11077413]
41. Metcalfe PD, Casale AJ, Kaefer MA, Misseri R, Dussinger AM, Meldrum KK, et al. Spontaneous bladder perforations: A report of 500 augmentations in children and analysis of risk. J Urol. 2006; 175(4):1466–1471. [PubMed: 16516023]
42. Kropp BP, Eppley BL, Prevel CD, Rippy MK, Harruff RC, Badylak SF, et al. Experimental assessment of small intestinal submucosa as a bladder wall substitute. Urology. 1995; 46(3):396–400. [PubMed: 7660517]
43. Badylak SF, Kropp B, McPherson T, Liang H, Snyder PW. Small intestinal submucosa: a rapidly resorbed bioscaffold for augmentation cystoplasty in a dog model. Tissue Eng. 1998; 4(4):379–387. [PubMed: 9916170]
44. Hu P, Meyers S, Liang FX, Deng FM, Kachar B, Zeidel ML, et al. Role of membrane proteins in permeability barrier function: uroplakin ablation elevates urothelial permeability. Am J Physiol Renal Physiol. 2002; 283(6):F1200–F1207. [PubMed: 12388410]
45. Schlager TA, Grady R, Mills SE, Hendley JO. Bladder epithelium is abnormal in patients with neurogenic bladder due to myelomeningocele. Spinal Cord. 2004; 42(3):163–168. [PubMed: 15001981]
46. Solway J, Forsythe SM, Halayko AJ, Vieira JE, Hershenson MB, Camoretti-Mercado B. Transcriptional regulation of smooth muscle contractile apparatus expression. Am J Respir Crit Care Med. 1998; 158(5):S100–S108. [PubMed: 9817732]
47. Kanematsu A, Ramachandran A, Adam RM. GATA-6 mediates human bladder smooth muscle differentiation: involvement of a novel enhancer element in regulating alpha-smooth muscle actin gene expression. Am J Physiol Cell Physiol. 2007; 293(3):C1093–C1102. [PubMed: 17626241]
48. Chiavegato A, Roelofs M, Franch R, Castellucci E, Sarinella F, Sartore S. Differential expression of SM22 isoforms in myofibroblasts and smooth muscle cells from rabbit bladder. J Muscle Res Cell Motil. 1999; 20(2):133–146. [PubMed: 10412085]
49. Qiu X, Montgomery E, Sun B. Inflammatory myofibroblastic tumor and low-grade myofibroblastic sarcoma: a comparative study of clinicopathologic features and further observations on the immunohistochemical profile of myofibroblasts. Hum Pathol. 2008; 39(6):846–856. [PubMed: 18400254]

50. Wu HY, Baskin LS, Liu W, Li YW, Hayward S, Cunha GR. Understanding bladder regeneration: smooth muscle ontogeny. J Urol. 1999; 162(3):1101–1105. [PubMed: 10458440]

51. Baskin LS, Hayward SW, Young P, Cunha GR. Role of mesenchymal-epithelial interactions in normal bladder development. J Urol. 1996; 156(5):1820–1827. [PubMed: 8863624]

52. Master VA, Wei G, Liu W, Baskin LS. Urothelium facilitates the recruitment and trans-differentiation of fibroblasts into smooth muscle in acellular matrix. Urology. 2003; 170(4):1628–1632.

53. Su ST, Huang HF, Chang SF. Encrusted Bladder Stone on Non-absorbable Sutures after a Cesarean Section: A Case Report. JTUA. 2009; 20(3):143–145.

54. Kong XT, Deng FM, Hu P, Liang FX, Zhou G, Auerbach AB, et al. Roles of uroplakins in plaque formation, umbrella cell enlargement, and urinary tract diseases. J Cell Biol. 2004; 167(6):1195–1204. [PubMed: 15611339]

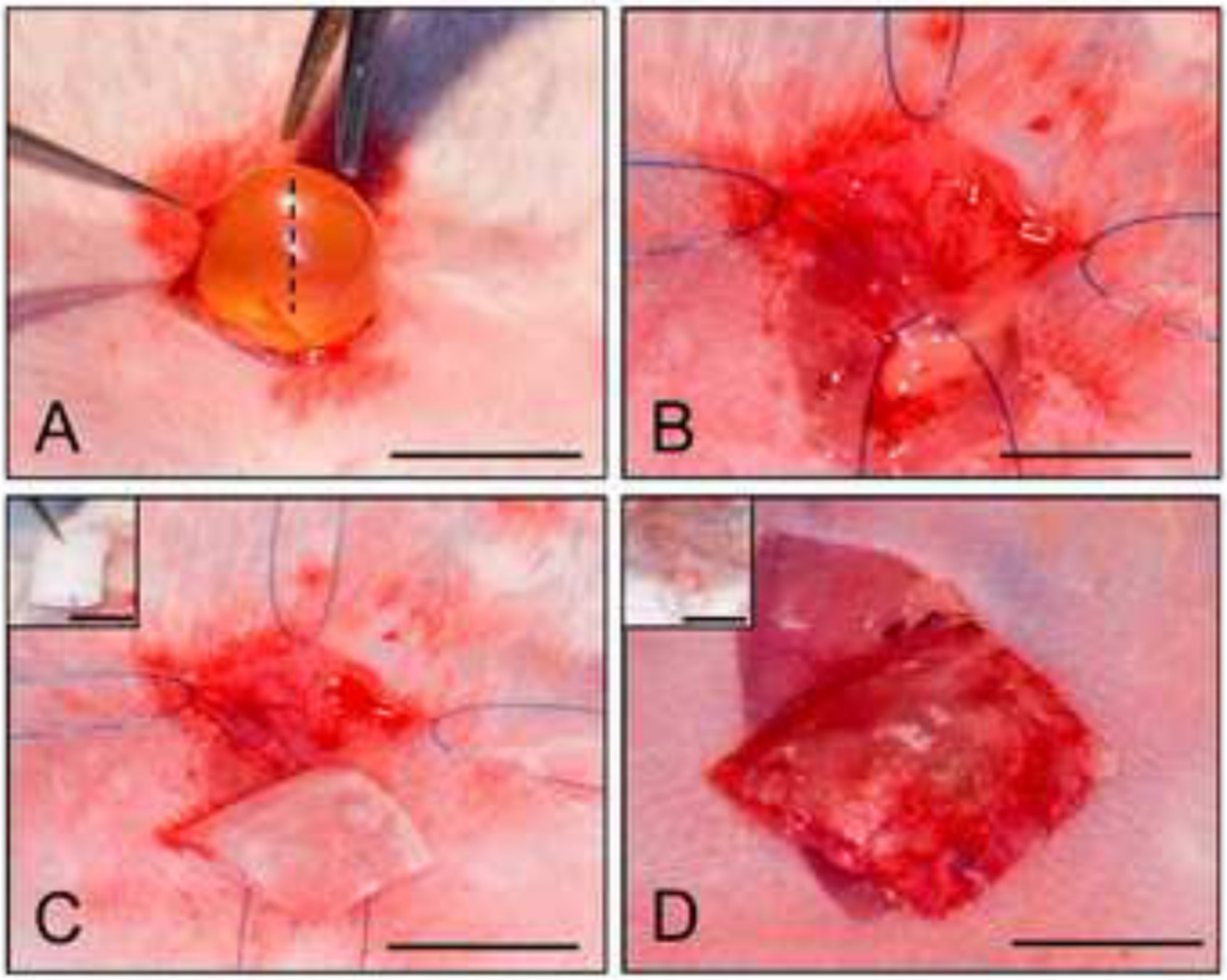

Figure 1. Murine bladder augmentation model

Photomicrographs of various surgical stages of gel spun silk matrix implantation. [**A**] Abdominal incision and extrusion of bladder. Hashed line denotes defect site. [**B**] Cystotomy and exposure of the bladder lumen. [**C**] Scaffold tailored to area of the defect site. Inset: Initial tubular configuration of matrix following fabrication. [**D**] Integration of the implant into the bladder wall. Inset: Placement of bladder into the abdominal cavity and surgical closure of the defect site. [**A, C**], scale bar = 5 mm. [**B, D**], scale bar = 3 mm. [**C, D** Insets], scale bar = 6 mm and 1.5 cm, respectively.

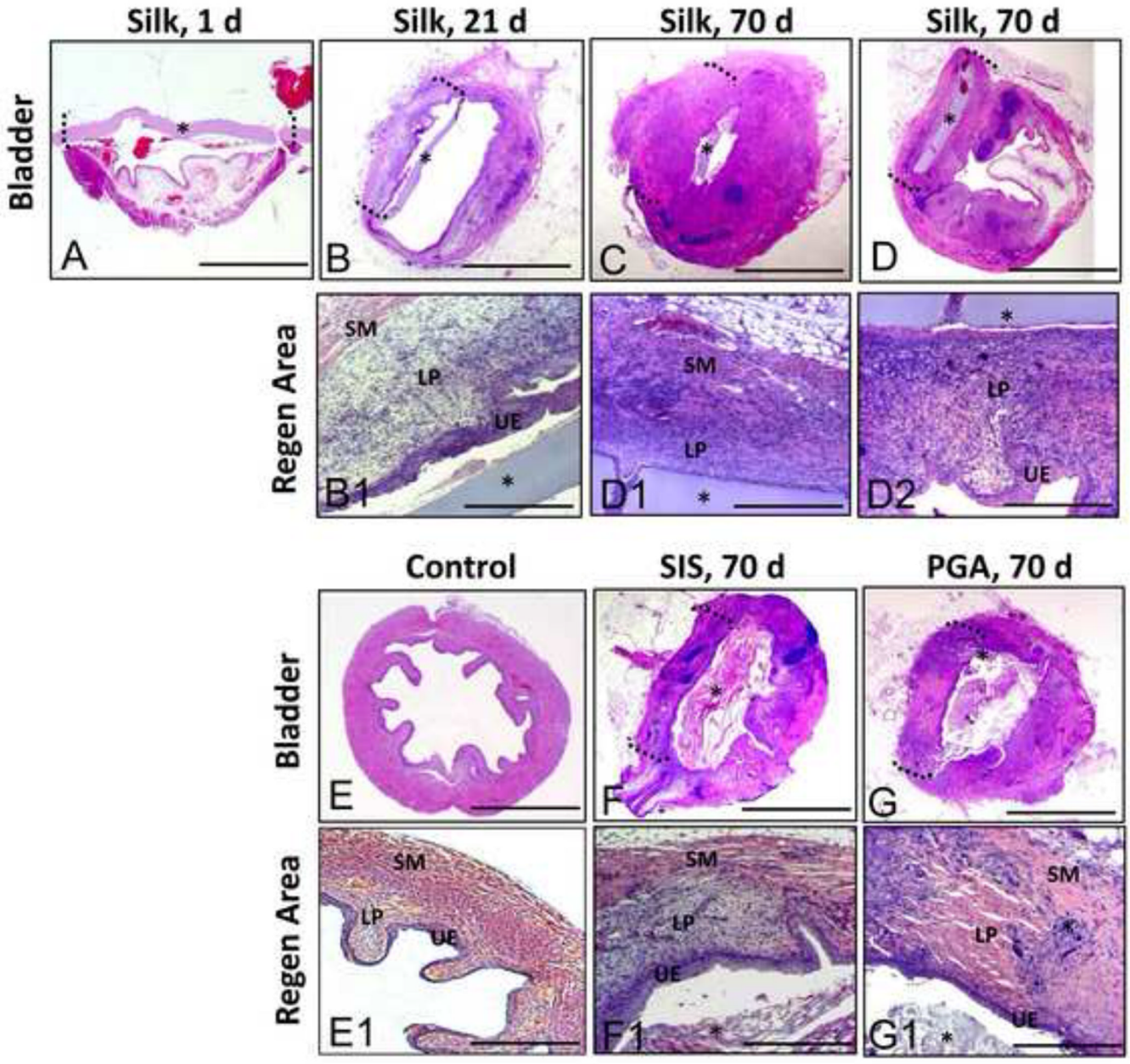

Figure 2. Hematoxylin and eosin analysis of bladder defect regeneration

Photomicrographs of total [**A–G**] and magnified [**A1-G1**] non surgical controls and bladders augmented with different scaffold groups over the course of the 70 d implantation period. UE = urothelium; LP = lamina propria, SM = smooth muscle compartments. (*) denotes scaffold fragments. Brackets denote area of tissue regeneration. [**A–G**], scale bar = 2.5 mm. [**A1-G1**], scale bar = 400 μm.

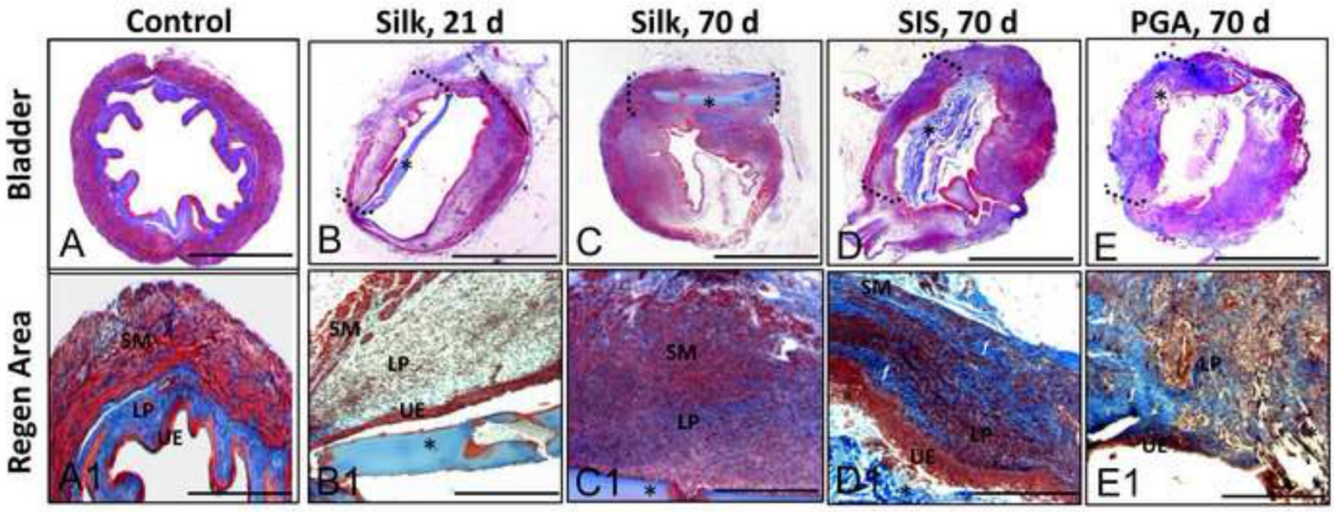

Figure 3. Masson's trichrome analysis of bladder defect regeneration

Photomicrographs of total [**A–G**] and magnified [**A1-G1**] non surgical controls and bladders augmented with different scaffold groups over the course of the 70 d implantation period. UE = urothelium; LP = lamina propria, SM = smooth muscle compartments. (*) denotes scaffold fragments. Brackets denote area of tissue regeneration. (*f*) = areas of fibrotic tissue. [**A–G**], scale bar = 2.5 mm. [**A1-G1**] scale bar = 400 μm.

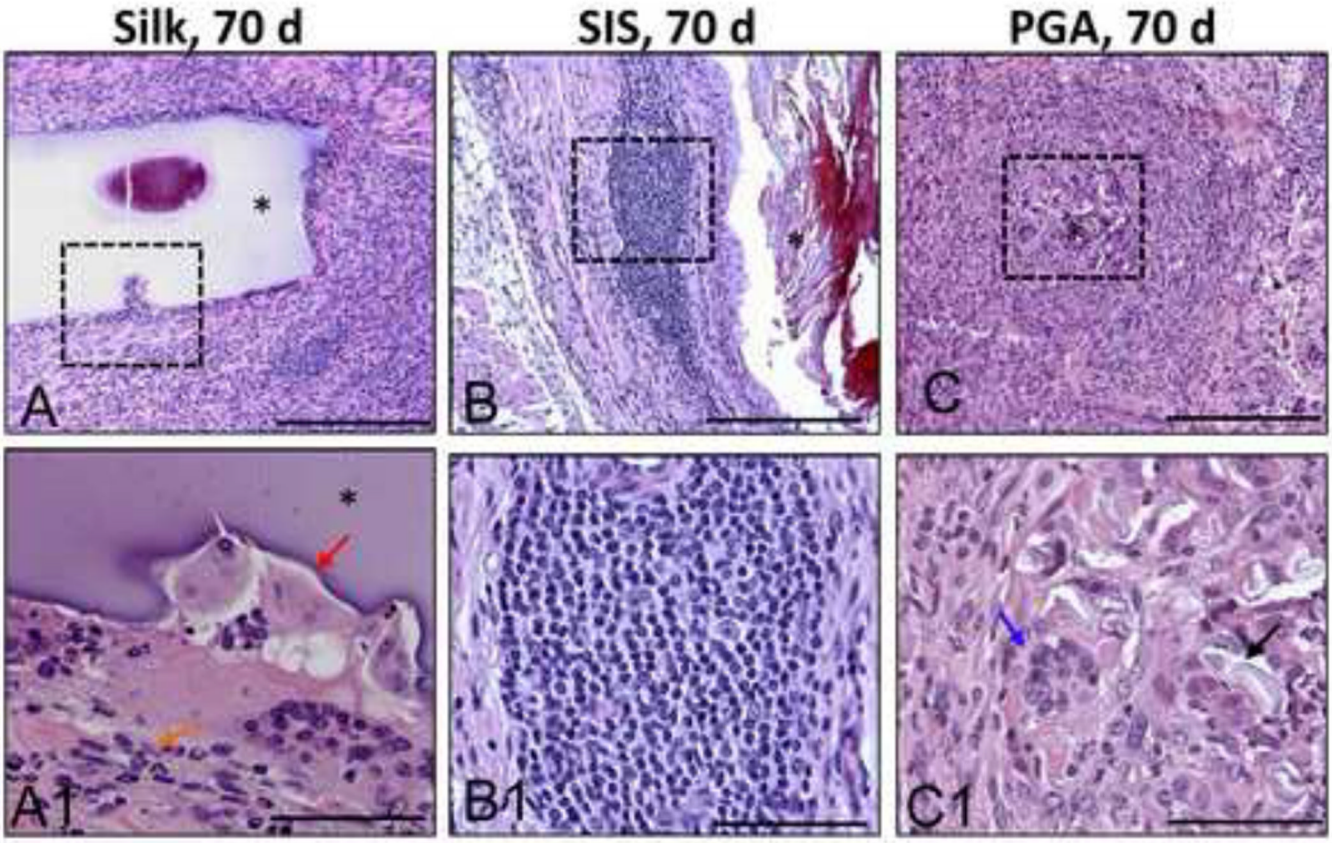

Figure 4. Inflammatory responses elicited by different scaffold groups at 70 d post-implantation

Photomicrographs of gross [**A–C**] and magnified [**A1–C1**] regenerated tissue area in augmented bladders following H&E staining. Magnified areas denoted by hashed boxes in [**A–C**]. [**A1**] Minimal acute inflammatory reaction elicited by silk matrix denoted by the presence of disperse eosinophil granulocytes (orange arrow). Focal area of mononuclear cell scaffold digestion (red arrow). [**B1**] Mild chronic inflammatory reaction exemplified by mobilized mononuclear cells in response to SIS implant. [**C1**] Severe chronic inflammatory reaction elicited by PGA matrix denoted by the presence of multi-nuclear giant cells (blue arrow) as well as foreign body encapsulation of scaffold remnants (black arrow). (*) denotes scaffold fragments. For [**A–C**] scale bar = 200 μm. For [**A1–C1**] scale bar = 50 μm.

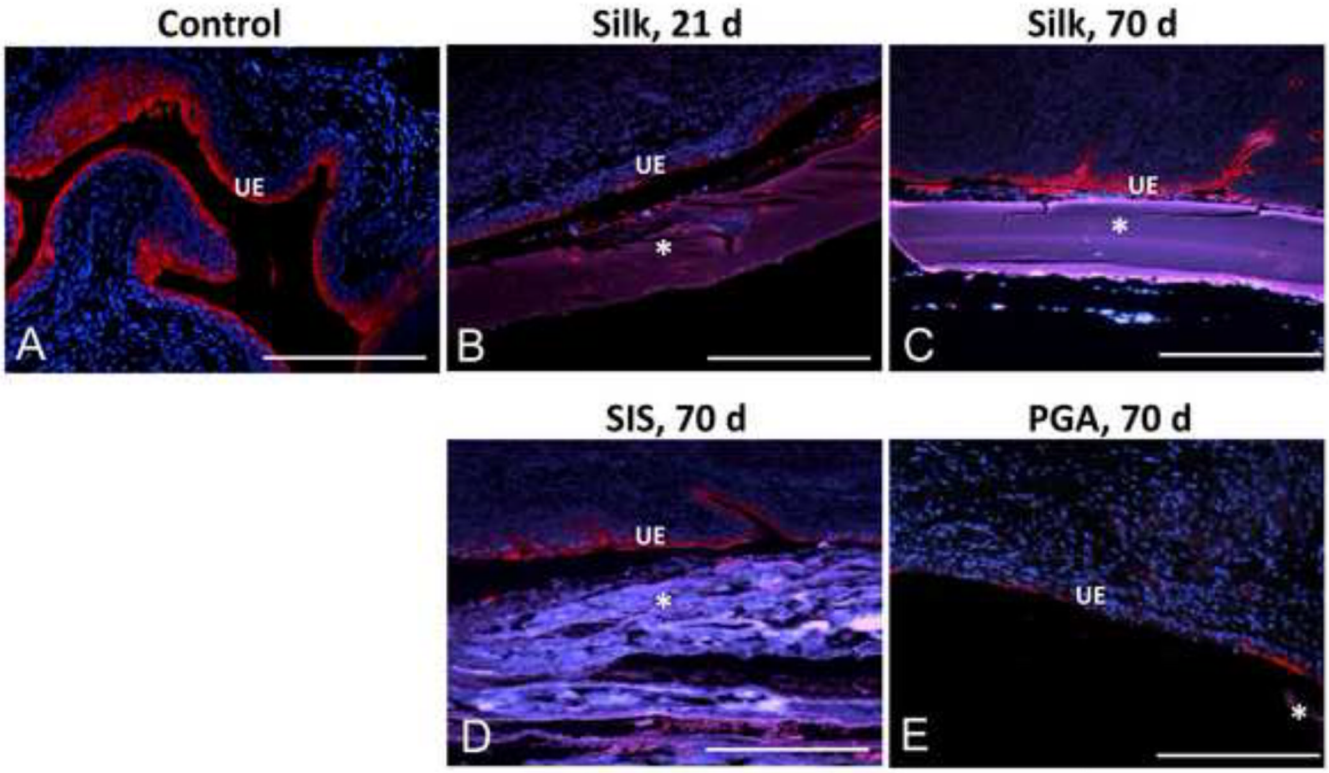

Figure 5. Extent of uroplakin expression in the regenerated urothelium supported by various scaffold groups

[**A–E**] Photomicrographs of immunohistochemical detection of pan-uroplakin expression (red, Cy3) in non surgical control and augmented bladders over the course of the 70 d implantation period. UE denotes urothelium. (*) denotes scaffold fragments. DAPI nuclear counterstain (blue). Scale bar for all panels = 420 μm.

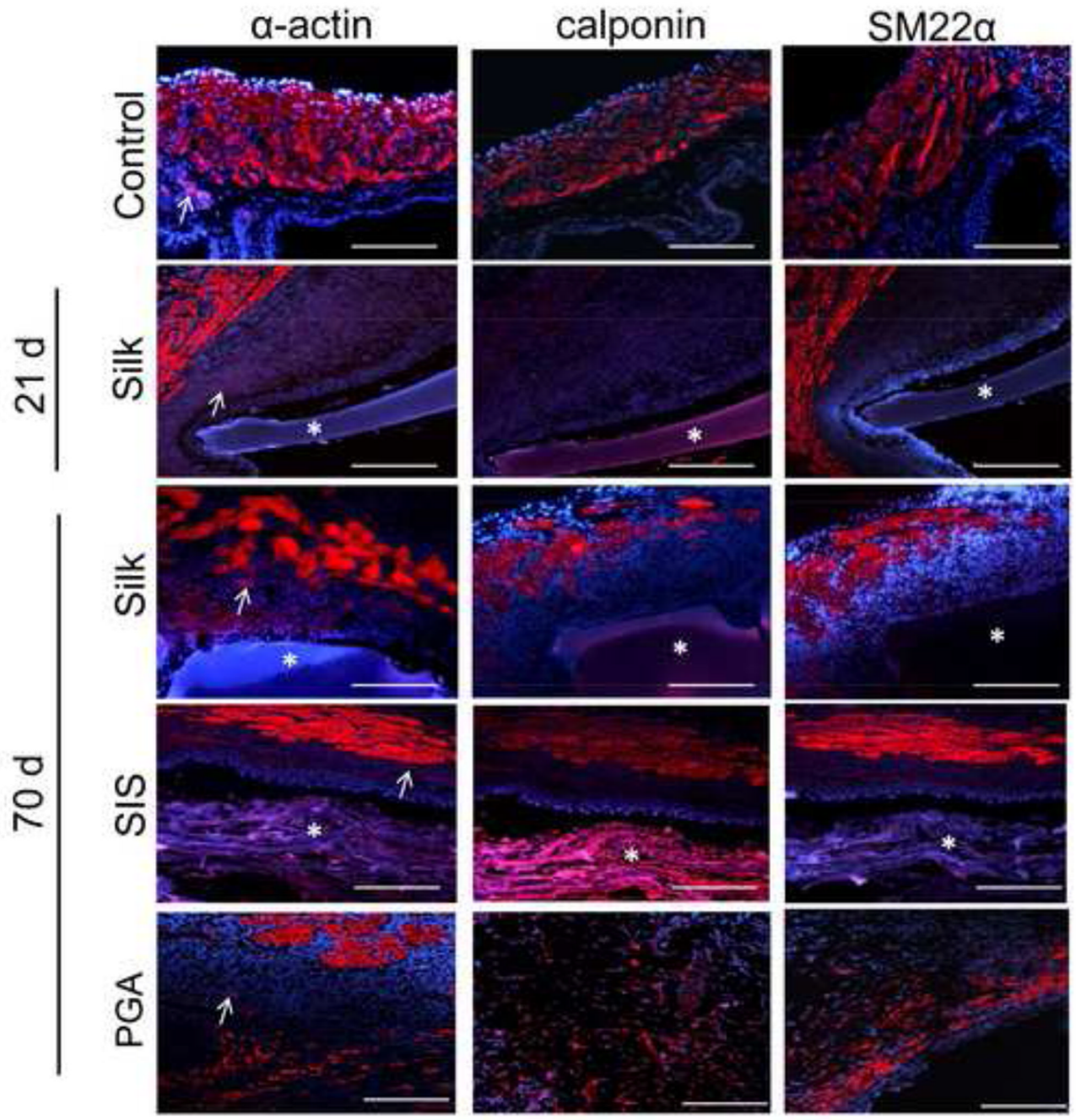

Figure 6. Extent of contractile protein expression in regenerated tissues following biomaterial incorporation

Photomicrographs of immunohistochemical detection of contractile protein (α-actin, calponin, and SM22α) expression (red, Cy3) in non surgical control and augmented bladders over the course of the 70 d implantation period. (*) denotes scaffold fragments. DAPI nuclear counterstain (blue). Arrows denote vessel structures in α-actin stained specimens. Scale bar for all panels = 420 μm.

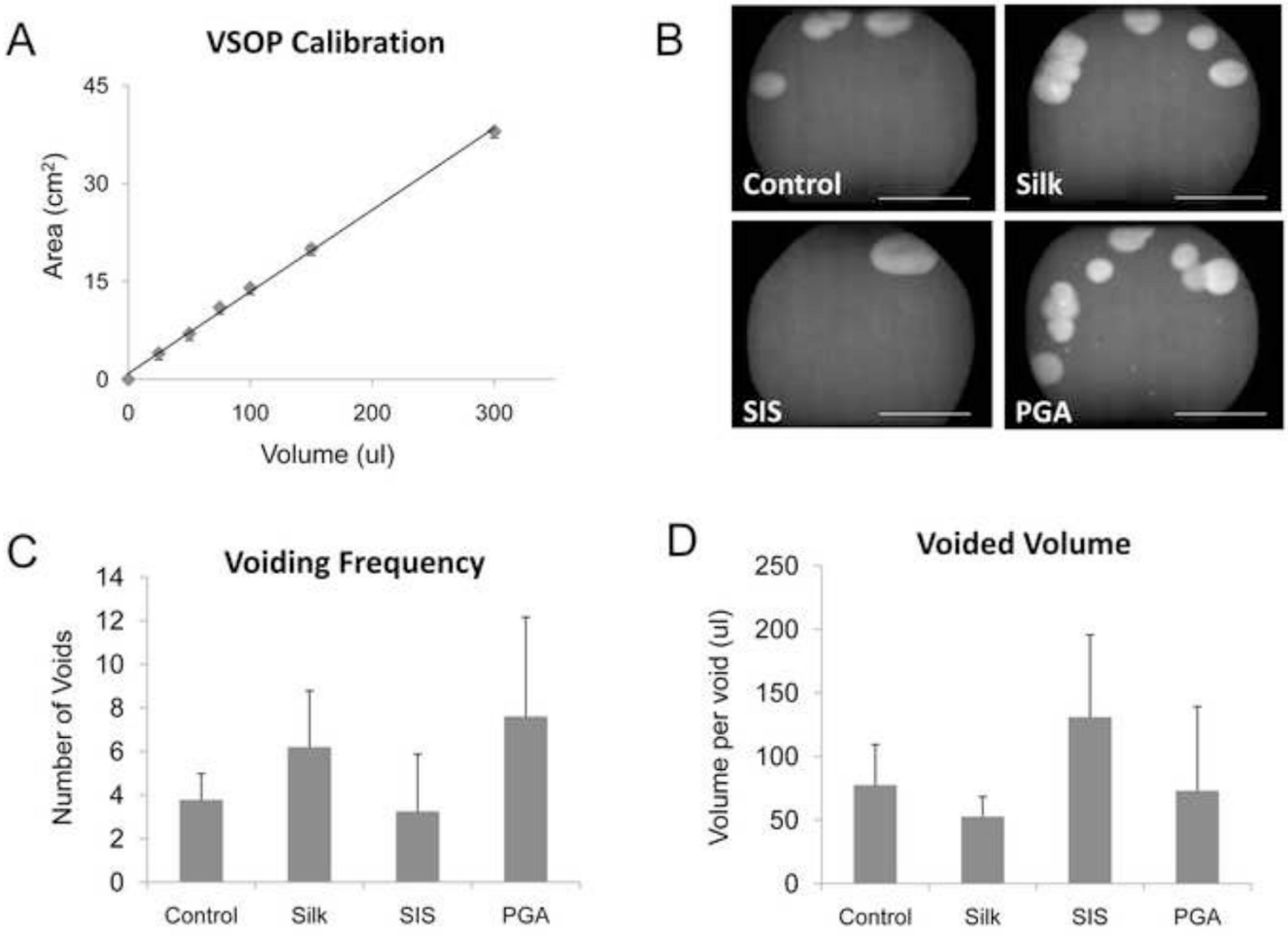

Figure 7. Voided stain on paper analysis of animals implanted with various scaffold groups following 42 d post-op

[**A**] Linear correlation between liquid volume and stained area on filter paper within the range of 25–300 μl, ($y = 0.125x + 0.898$, $R^2 = 0.9979$). [**B**] Photomicrographs of UV-enhanced voiding patterns on filter paper representative of each matrix group and non surgical controls. Scale bar = 9.5 cm. Comparison of voiding frequencies [**C**] and voided volume [**D**] between scaffold groups and control animals. For [**C, D**], data are expressed as means ± standard deviation.

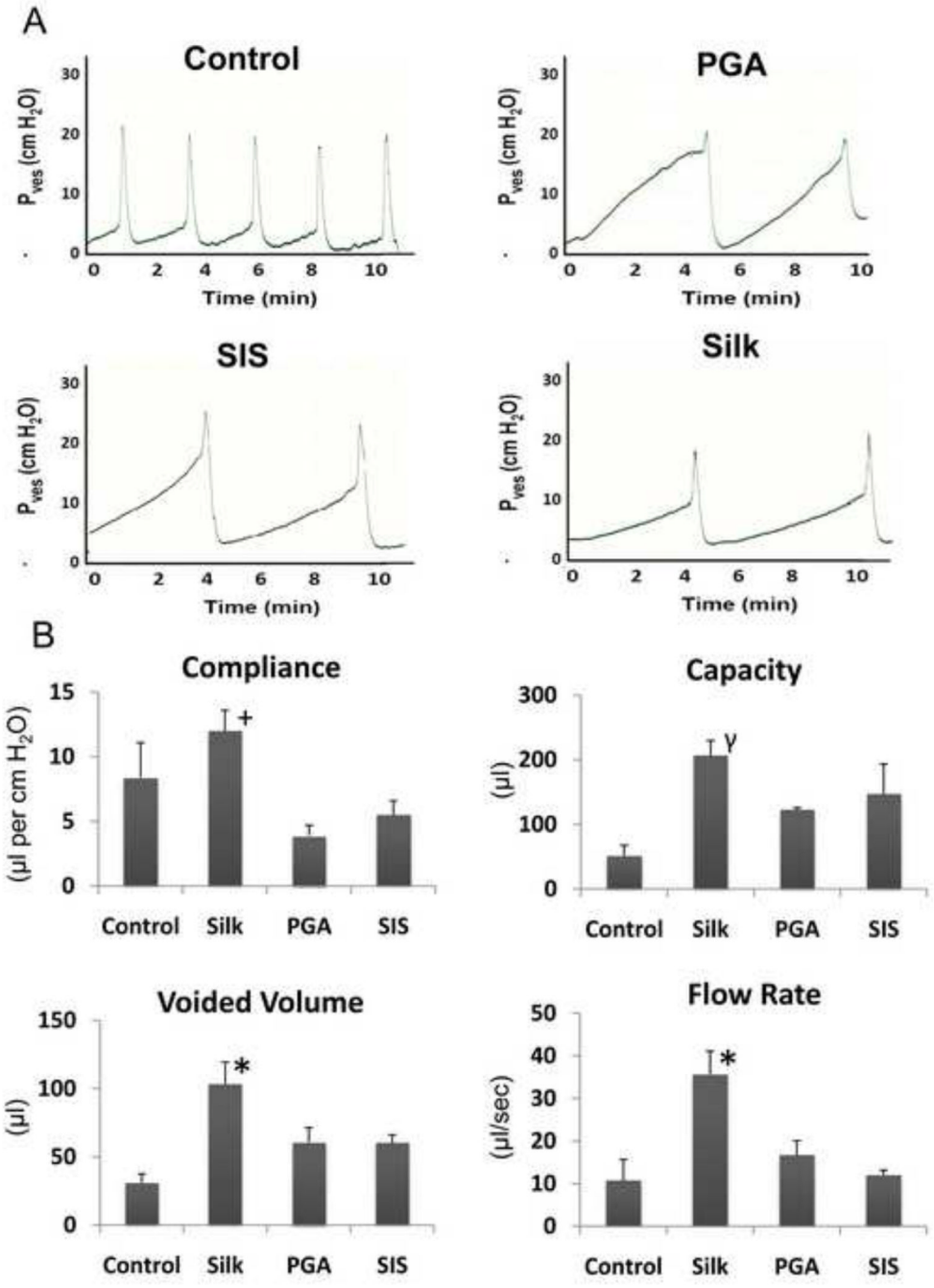

Figure 8. Cystometric analysis and quantification of urodynamic parameters in augmented bladders following 70 d post-implantation

[**A**] Representative cystometric tracings of voiding cycles displayed by non surgical controls, silk, SIS, and PGA implanted bladders. [**B**] Comparisons of urodynamic parameters including bladder compliance, capacity, voided volume, and flow rate between experimental groups displayed in [**A**]. (+) = $p>0.05$, compared to non surgical control. (γ) = $p<0.05$, compared to non surgical control. (*) = $p<0.05$, compared to all other groups. For [**B**], data are expressed as means ± standard deviation.

Table 1

Experimental design and analyses

Summary of type and time scale of analyses for each implant group.

Groups	Total number of animals analyzed	Survival rate (%) until planned euthanasia	Histology (1,21,70 d)	VSOP (42 d)	Urodynamics (70 d)
Control	12	100	3(70)	5	4
Silk	17	82	1(1), 3(21), 3(70)	5	4
PGA	7	71	2(70)	5	2
SIS	6	66	2(70)	4	2